Recent Advance in LHD Experiment

O. Motojima 1), N. Ohyabu 1), A. Komori 1), O. Kaneko 1), H. Yamada 1), K. Kawahata 1), Y. Nakamura 1), K. Ida 1), T. Akiyama 2), N.Ashikawa 1), W.A. Cooper 3), A. Ejiri 4), M. Emoto 1), N. Ezumi 5), H. Funaba 1), A. Fukuyama 6), P. Goncharov 7), M. Goto 1), H. Idei 1), K. Ikeda 1), S. Inagaki 1), M. Isobe 1), S. Kado 8), H. Kawazome 6), K. Khlopenkov 1), T. Kobuchi 1), K. Kondo 6), A. Kostrioukov 1), S. Kubo 1), R. Kumazawa 1), Y. Liang 1), J.F. Lyon 9), A. Mase 10), S. Masuzaki 1), T. Minami 1), J. Miyazawa 1), T. Morisaki 1), S. Morita 1), S. Murakami 1), S. Muto 1), T. Mutoh 1), K. Nagaoka 1), Y. Nagayama 1), N. Nakajima 1), K. Nakamura 11), H. Nakanishi 1), K. Narihara 1), Y. Narushima 1), K. Nishimura 1), N. Nishino 12), N. Noda 1), T. Notake 13), H. Nozato 4), S. Ohdachi 1), Y. Oka 1), H. Okada 6), S. Okamura 1), M. Osakabe 1), T. Ozaki 1), B.J. Peterson 1), A. Sagara 1), T. Saida 7), K. Saito 1), S. Sakakibara 1), M. Sakamoto 11), R. Sakamoto 1), M. Sasao 1), K. Sato 1), M. Sato 1), T. Seki 1), T. Shimozuma 1), M. Shoji 1), H. Suzuki 1), Y. Takeiri 1), N. Takeuchi 13), N. Tamura 1), K. Tanaka 1), M.Y. Tanaka 1), Y. Teramachi 14), K. Toi 1), T. Tokuzawa 1), Y. Tomota 15), Y. Torii 13) K. Tsumori 1), K.Y. Watanabe 1), T. Watari 1), Y. Xu 1), I. Yamada 1), S. Yamamoto 13), T. Yamamoto 13), M. Yokoyama 1), S. Yoshimura 1), Y. Yoshimura 1), M. Yoshinuma 1), N. Asakura 16), T. Fujita 16), T. Fukuda 16), T .Hatae 16), S. Higashijima 16), A. Isayama 16), Y. Kamada 16), H. Kubo 16), Y. Kusama 16), Y. Miura 16), T. Nakano 16), H. Ninomiya 16), T. Oikawa 16), N. Oyama 16), Y. Sakamoto 16), K. Shinohara 16), T. Suzuki 16), H. Takenaga 16), K. Ushigusa 16), T. Hino 17), M. Ichimura 18), Y. Takase 4), F. Sano 6), H. Zushi 11), T. Satow 1), S. Imagawa 1), T. Mito 1), I. Ohtake 1), T. Uda 1), K. Itoh 1), K. Ohkubo 1), S. Sudo 1), K. Yamazaki 1), K. Matsuoka 1), Y. Hamada 1), M. Fujiwara 1).

1) National Institute for Fusion Science 1), Toki, Gifu, Japan
2) Research Laboratory for Nuclear Reactors, Tokyo Institute of Technology, Japan
3) CRPP, EPFL), Lausanne, Switzerland
4) Graduate School of Frontier Sciences, The University of Tokyo, Tokyo, Japan
5) Nagano National College of Technology, Nagono, Japan
6) Graduate School of Energy Science, Kyoto University, Uji, Japan
7) Department of Fusion Science, School of Mathematical and Physical Science, Graduate University for Advanced Studies, Hayama, Japan
8) High Temperature Plasma Center, The Univ. of Tokyo, Tokyo, Japan
9) Ork Ridge National Laboratory, Tennessee, USA
10) Advanced Science and Technology Center for Cooperative Research, Kyushu Univ. Japan
11) Research Institute for Applied Mechanics, Kyushu University, Fukuoka, Japan
12) Faculty of Engineering, Hiroshima Univ., Hiroshima, Japan
13) Department of Energy Engineering and Science, Nagoya University, Nagoya, Japan
14) The Polytechnic University, Japan
15) Department of Engineering, Ibaraki Univ. Japan
16).Naka Fusion Research Institute, JAERI, Japan
17) Faculty of Engineering, Hokkaido University, Sapporo, Japan
18).University of Tsukuba, Tsukuba, Japan

e-mail contact of main author: motojima@LHD.nifs.ac.jp

Abstract: In the first four years of LHD experiment, several encouraging results have emerged, the most significant of which is that MHD stability and good transport are compatible in the inward shifted axis configuration. The observed energy confinement at this optimal configuration is consistent with ISS95 scaling with an enhancement factor of 1.5. The confinement enhancement over the smaller heliotron devices is attributed to the high edge temperature. We find that plasma with an average beta of 3 % is stable in this configuration even though the theoretical stability conditions of Mercier modes and pressure driven low n modes are violated. In the low density discharges heated by NBI and ECR heatings, ITB(internal transport barrier) and an associated high central temperature (> 10 keV) are seen. The radial electric field measured in these discharges is positive (electron root) and expected to play a key role in the formation of the ITB. The positive electric field is also found to suppress the ion thermal diffusivity as predicted by neoclassical transport theory. The width of the externally imposed island (n/m=1/1) is found to decrease when the plasma is collisionless with finite beta and it increases when the plasma is collisional. The ICRF heating in LHD is successful and a high energy tail (up to 500keV) has been detected for minority ion heating, demonstrating good confinement of the high energy particles. The magnetic field line structure unique to the heliotron edge configuration is confirmed by measuring the plasma density and temperature profiles on the divertor plate. A long pulse (2minute) discharge with an ICRF power of 0.4 MW has been demonstrated and energy confinement characteristics are almost the same as those in short pulse discharges.

1.Introduction

In the first four years of the Large Helical Device (LHD) experiment, we have made the necessary progress in achieving high quality plasmas [1-10]. As indicated by the presently achieved plasma parameters listed in Table I, recently high central electron temperatures of 10 keV have been obtained by localizing the ECH power deposition (a total of 1.2 MW) within $\rho = 0.2$ [11,12]. One of the most important achievement in the CHS [13] and LHD experiments has been to resolve favorably the conflict between stability and confinement. The inward shifted configurations are ideal in terms of particle orbit and consequently the neoclassical loss [14] and volume of the confinement region. On the other hand they have been predicted to have poor MHD stability. The experiments demonstrate that LHD helical plasmas in the inward shifted configuration are stable despite of the unfavorable prediction by ideal linear MHD stability theory. Also it has been shown that the heat diffusivity of anomalous transport in this configuration is even lower than that in the outward shifted configuration having theoretically better MHD stability. Enhancement of the energy confinement is the key to advancing the LHD experiment. We have found that with central deposition of ECH power, an ITB (Internal Transport Barrier) appears in the low density, beam heated discharges, which provided significant impetus to the LHD experimental program. The LHD is a heliotron type device with an intrinsic divertor. It is the largest superconducting fusion device, with its specifications listed in Table II. The major goal of the LHD experiment is to demonstrate the high performance of helical plasmas in a reactor relevant plasma regime. The LHD experiment began in March 1998 after its intensive eight-year construction period. In the present LHD experiments, plasmas are heated by NBI, ICRH and ECH systems and the maximum powers absorbed by the plasma have been gradually increased. A list of available power is shown in Table II. Plasma generation is normally initiated by ECH power and then the main power is added to heat the plasma. With good wall conditions, however, plasma initiation or start-up is possible by simple injection of the NBI power [15]. With this start-up, we can operate low field discharges, independently of the ECH resonance conditions. Carbon divertor tiles are used to handle the heat flux from the core. Stainless protection plates cover the vacuum vessel. The wall conditioning is mainly done by glow discharges and vessel baking (100° C). In the following the recent results of the LHD experiment are summarized for several important research subjects, i.e., heat transport, stability and long pulse operation.

Table I Achieved plasma parameters

	T	n_e
High Electron Temperature	10 keV	0.6×10^{19} m^{-3}
High Ion Temperature	5.0 keV	0.7×10^{19} m^{-3}
High Confinement	1.3 keV	4.8×10^{19} m^{-3}
$\tau_E = 0.36$ s, $nT\tau_E = 2.2\times 10^{19}$ keV m^{-3} , $P_{abs} = 1.5$ MW,		
Maximum Stored Energy	Wp = 1.2 MJ	
Highest Beta	$\langle\beta\rangle = 3.2$ % at B = 0.5 T	
Maximum Density	1.5×10^{20} m^{-3}	

Table II LHD device parameters and heating power used in the experiment.

Major radius	3.9 m	B_o	2.9 T
Coil minor radius	0.975 m	$\iota(0) / \iota(a)$	0.4 / 1.3
Plasma radius	~0.6 m	HeatingPower(absorbed)	
l/m	2 / 10	NBI	9.0 MW
α (pitch modulation)	0.1	ECRH	1.7 MW
Helical ripple	0.2	ICRF	2.7 MW

2. Heat Transport of the LHD plasmas

2.1. Global Energy Confinement of LHD Plasma

The energy confinement times in the LHD inward shifted discharges (R_{ax} = 3.6 m) are consistent with the ISS95 scaling [16] with an enhancement factor of ~1.5 and are comparable to those in ELMy H-mode tokamaks discharges with q = 4.5 [17]. They are a factor of 2 higher than those of smaller heliotron devices such as CHS, Heliotron E, and ATF. This enhancement is attributed to high edge temperature, as described below [18,19]. Further enhancement of the energy confinement and hence suppression of the plasma turbulence are required for high performance of the LHD plasmas. The neoclassical transport loss (ripple loss) is also a concern for the LHD type devices. Numerical calculation shows that the inward shifted configuration (R_{ax} = 3. 5-3.6 m) has good particle orbit properties [15], i.e., deviation of the deeply trapped particle orbit from the magnetic surface is small and the deviation becomes larger with increasing R_{ax} ,reaching a fraction of the minor radius at R_{ax} = 3.75-3.9 m.

The dependence of the energy confinement on the position of the magnetic axis is studied [20].The enhancement factor over the ISS95 scaling is found to be sensitive to variation in the magnetic axis position (R_{ax}). It is optimum at R_{ax} = 3.55-3.6 m and decreases with increasing R_{ax}. For R_{ax} = 3.9 m, it is as small as 0.6. Furthermore, strong deterioration of the confinement occurs for R_{ax} = 3.75 and 3.9 m when the plasma becomes collisionless ($\nu^* < 1$). This is believed to be due to neoclassical transport (ripple loss). For inward shifted discharges with low neoclassical transport, the enhancement factor is independent of ν^* and hence the anomalous transport dominates over the neoclassical transport.

2.2. Electron Temperature Profile in LHD Discharges

The shape of the electron temperature profile does not vary much over a wide range of the density ($1.5\times10^{19}m^{-3} < n < 9\times10^{19}m^{-3}$) when the island size (n/m=1/1) is minimized by the correction coils in the discharges (P = 8 MW, B = 2.75T, R_{ax} = 3.6m). Fig. 1(a) shows electron temperature profiles at two different densities ($3.5\times10^{19}m^{-3}$, $7\times10^{19}m^{-3}$). The shapes of the

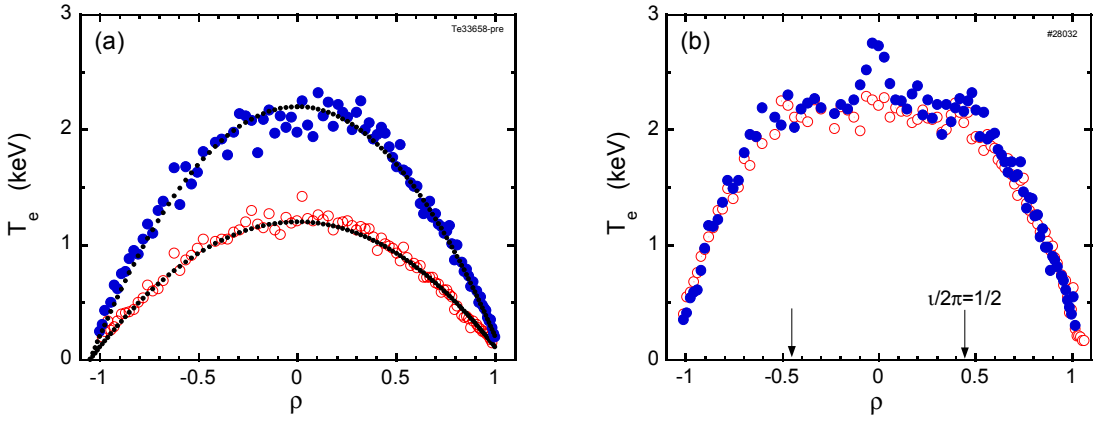

Fig. 1. (a). Shape of the electron temperature profile. The profile shapes for the discharges with two different densities (● $3.5\times10^{19}m^{-3}$, o $7\times10^{19}m^{-3}$) are nearly identical. The curves (……) are : $T_e = T_e(0)[1-(\rho/1.05)^2]$. B = 2.75 T, R_{ax} = 3.6m. (b). (o): flattening of the core electron temperature profile for low density, ctr-beam heated discharges. . (●): with modest ECRH power (300kW) in the core, a small ITB appears in the center. n =1.35×10^{19} m^{-3}

temperature profiles are similar and they are close to a parabolic profile if plotted in terms of ρ (the normalized radius). The parabolic profile is fairly broad and leads to better normalized global confinement compared with smaller heliotron devices with peaked profiles [18,19]. The broadness of the profile is found to be similar to those of a comparable H-mode tokamak such as ASDEX-U[21] [For ASDEX-U, T_e (0.4)/T_e (0.8) is ~1.8 and for LHD it is ~2.0].

In the low density ($n < 1.5\times10^{19}m^{-3}$) counter(ctr)-beam heated discharges (R_{ax} = 3.5, 3.6 m), however, core flattening of the profile occurs, deviating significantly from the parabolic profile as shown in Fig.1(b) [22]. Part of reason for the flattening is that a smaller fraction of power is deposited in the core region compared with the co-beam heated discharges which exhibit a peaked temperature profile even at such low density. But profile flattening persists even if the localized ECH power is deposited in the core and hence dominates NBI power in the core power balance. We find that flattening is localized within the $\iota/2\pi = 1/2$ surface. The effective electron thermal diffusivity χ_{eff} in the core is very high more than 50 m^2s^{-1}(here χ_{eff} is defined as $q = n\,\chi_{eff}\,\nabla\,T_e$). Ripple transport without radial electric field causes large χ at high temperature, but it is as small as 0.8 m^2s^{-1} for the temperature of the present case (T_e =2.2 keV). Thus it is difficult to explain this level of rapid transport without invoking some kind of structural confinement loss .

2.3. Internal Transport Barrier (ITB)

The temperature profile in the normal LHD discharge is close to parabolic. In the low density ($n < 1.5\times10^{19}m^{-3}$) counter(ctr)-beam heated discharges (R_{ax} = 3.53m), however, flattening of the profile occurs in the core region within the $\iota/2\pi = 1/2$ surface. With higher ECH power, a bump (a small ITB) appears in the center[Fig.1(b))]. Further higher ECH power leads to complete formation for the ITB [13]. There is a clear ECH power threshold for a complete formation of the ITB as shown in Fig. 2. At P_{ECH} = 180kW (R_{ax}= 3.5 m), there is a small bump in the flattened core and at P_{ECH} = 280kW, a complete formation of the ITB occurs. The power threshold increases with increasing density. The foot location of the ITB defined as the location of the jump in ∇T is typically around ρ ≈ 0.2 and increases slightly with P/n.

Core heat transport in the low density co-beam heated discharges is quite different from that of the ctr-beam case [22]. Core flattening does not occur and its profile is even slightly peaked than the parabolic profile. With added ECH power, the central temperature increases and a much wider ITB forms, as shown in Fig. 3. The jump in ∇T is much smaller at the foot point compared with ctr-beam case, but the central temperature is comparable. The foot point is located around the ρ ≈ 0.5 surface. Outside the footpoint, the profile is close to the parabolic profile. Unlike ctr-beam case, a clear ECH power threshold for the ITB does not

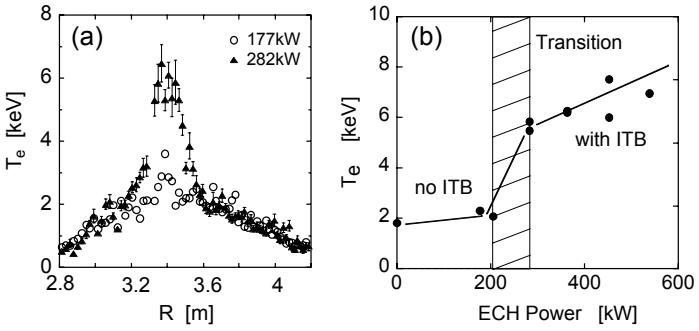

Fig.2. (a) A typical ITB electron temperature profile for the ctr-beam and ECRH heated discharges.
(b) A clear ECH power threshold for ITB formation for ctr-beam heated discharges.

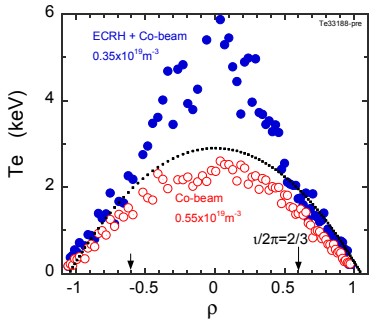

Fig. 3. (•) electron temperature profile during co-beam and ECH heatings. (o): the profile during co-beam heating. The dotted curve is T_e = 2.9 [1-(ρ/1.05)^2]

seem to exist.

A natural question arises, as to why the temperature profile or ITB width differ between the co and ctr-beam heated discharges. A co-(ctr-) beam drives positive (negative) Ohkawa current of > 60 kA (sign convention of the current is that positive (negative) current increases (decreases) the rotational transform). The core ι-profile is sensitive to this current and hence influences the core transport. We find, however, that there exists strong beam effects on the core transport and the ITB formation. For example, the location of the ITB footpoint during co-beam plus ECH heating phase is around ρ = 0.5, being insensitive to current amplitude and direction. In the LHD Experiment, the co-beam phase with negative current is created by being preceded by a ctr-beam phase. The counter-beam is found to have unfavorable effects on ITB, i) existence of a power threshold for ITB formation, (ii) core flattening of the electron temperature profile below the threshold power, (iii) narrow ITB (ρ < 0.2), surrounded by a flattening region, (iv) with high ctr-beam power, core plasma tends to collapse like a sawtooth oscillation in tokamaks. On the other hand, co-beam has favorable effects (i) broader profile (ρ < 0.5), (ii) no clear power threshold, (iii) furthermore the externally imposed large island (n/m=1/2) tends to be suppressed. These observations support our working hypothesis that some kind of structural confinement loss appears in the ctr-beam heated low density discharges. We also observe that the amplitude of the magnetic fluctuations in the form of a burst is high during the ctr beam heated phase and is low during the co-beam phase. Thus the observed fluctuations may play a key role in the core transport mentioned above. Further study will be needed for deeper understanding of the observed transport.

2.4. Role of Radial Electric Field in the transport of the LHD Plasmas

The radial electric field (E_r) is required for confinement of collisionless helical plasmas. Its shear is believed to be the important parameter to suppress the plasma turbulence, which causes the anomalous heat loss

The transition from ion (negative radial electric field) root to electron (positive radial electric field) root is observed at the low density of 0.4 – 1.0 x $10^{19}m^{-3}$ in the beam heated LHD discharges. The E_r was negative at the electron density higher than 1.0 x $10^{19}m^{-3}$, while it became positive especially near the plasma edge at the low density below 1.0 x $10^{19}m^{-3}$. Fig. 4 shows the ion temperature and E_r profiles for ion root and electron root cases in the standard discharges (R_{ax}=3.75 m) [23]. In the LHD, the density profile is flat, slightly inverted for the low-density discharges. The ion temperature profile, particularly temperature gradients in the edge are quite different (Fig. 4(a)). The electron temperatures are higher than ion temperatures and are nearly identical for two cases. From the profile data, the E_r can be estimated by neoclassical transport theory and the estimated values qualitatively agree with the measured

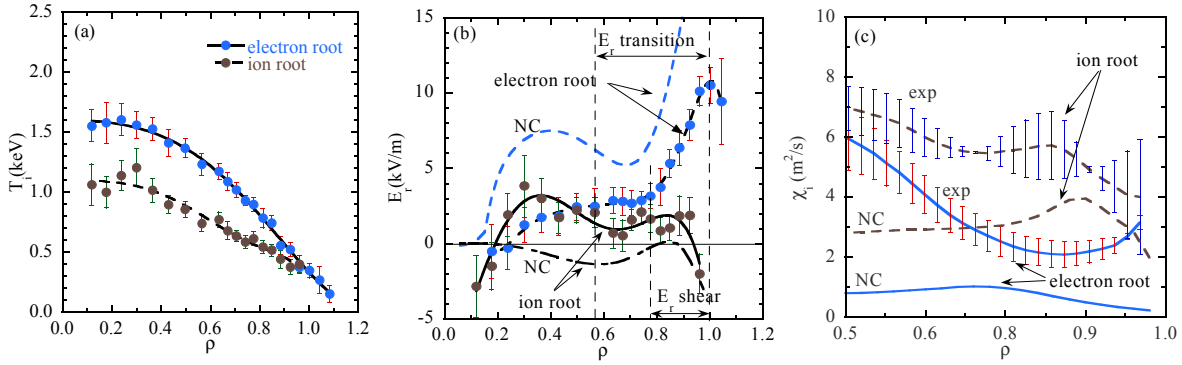

Fig. 4. Radial profiles of (a) ion temperature, (b) radial electric field, (c) ion thermal diffusivity are plotted for the electron root (n=0.7×$10^{19}m^{-3}$)(blue circle) and ion root (n=1.0×$10^{19}m^{-3}$) (black circles) plasmas.

values (Fig. 4(b)). The ion temperature gradient for the electron root (lower density) case is substantially higher than that of the ion root (higher density) case in the outer region ($\rho > 0.6$)(Fig. 4 (a)) where high positive E_r (3-10 keV/m) is seen (Fig. 4(b)). Thus ion thermal diffusivity for the electron root is lower in the outer region (Fig .4(c)). High E_r in the electron root suppresses the neoclassical ion transport. Such suppression is not observed for the inward shifted configuration (R_{ax} = 3.6m), in which neoclassical transport is low and hence the anomalous transport easily dominates over the neoclassical transport.

With combined heating of NBI and ECH in the low density discharges, an ITB appears and the measured E_r is found to be positive in the entire region and its value is approximately a half of the neoclassical prediction. Even though the transition from ion to electron root in the core does not trigger the ITB formation, a positive feedback cycle is plausible, i.e., due to neoclassical effect, higher electron temperature gradient leads to higher E_r and hence higher shear of the E_r, which in turn suppresses the plasma turbulence and improve confinement, leading to higher temperature gradient [24]. The electron thermal diffusivity is observed to be reduced significantly when the ITB forms. But it is a factor of 10 higher than the neoclassical value which takes into account the measured E_r.

3. Stability of the LHD Plasmas

3.1. Stability of pressure driven MHD instabilities in the LHD

We have achieved averaged beta (<β>) of ~ 3 % at B = 0.5 T[25]. The <β> value was limited by the available heating power. It is achieved in the inward shifted configuration (R_{ax} ~ 3.60 m), in which the magnetic hill exists in the entire region. Fig. 5(a) shows Mercier and low n mode unstable regions and LHD data points in a parameter space ($d\beta/d\rho_{at\ \rho=0.5}$ and <β>). The mode (n/m=1/2) is primarily driven by the normalized pressure gradient ($d\beta/d\rho$) at the $\iota/2\pi = 0.5$ surface (which approximately corresponds to $\rho = 0.5$)[20]. The stability of the low n mode is evaluated by the three-dimensional MHD stability analysis code TERPSICHORE [26] with the assumption of the pressure profile form, $P(\rho) = (1-\rho^M)^N$. Most of the data points below 2% of <β> are in the Mercier unstable region, but in the outside of the low n unstable region, indicating that the plasma may naturally adjust its pressure gradient in such a way as to avoid a presumably violent low n mode. The n/m=1/2 mode appears when <β> exceeds about 0.3 % and its amplitude increases rapidly until <β> reaches 2.3 %. Beyond 2.3 % of <β>, it

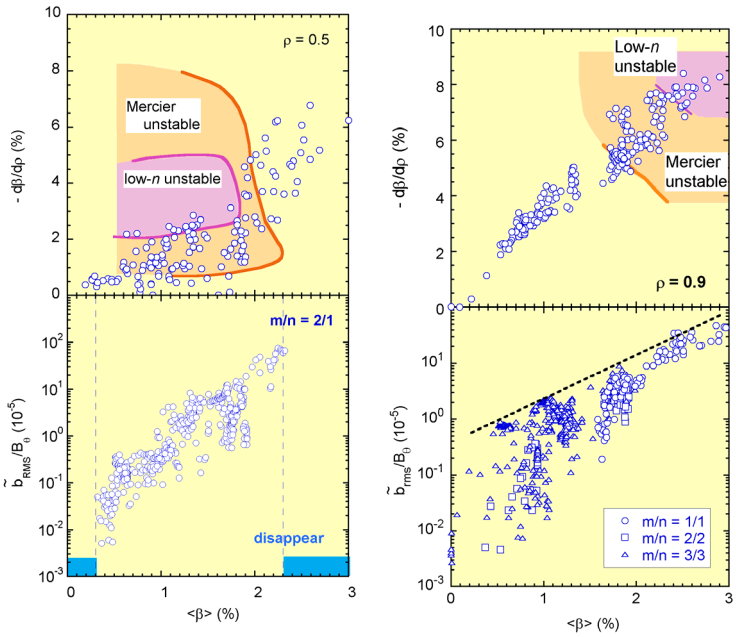

Fig. 5. (a) Evolution of the normalized pressure gradient ($d\beta/d\rho$) at $\rho = 0.5$ and amplitude of magnetic fluctuation (n/m=1/2) with increasing β. Mercier unstable and low n unstable regimes are illustrated for comparison. (b) Evolution of the normalized pressure gradient t($d\beta/d\rho$) at $\rho = 0.9$ and amplitude of magnetic fluctuation (n/m=1/1,2/2,3/3) with increasing β. Mercier unstable and low n unstable regimes are illustrated for comparison.

disappears, entering the second stability regime of the n/m=1/2 mode. Mode appearance and disappearance are consistent with the predictions of the linear ideal MHD theory.

Other critical modes reside around the $\iota/2\pi = 1$ surface (ρ=0.9). Fig. 5(b) depicts the unstable regime in $d\beta/d\rho_{at\ \rho=0.9}$ and $<\beta>$ space. When $<\beta>$ is low (below 1.8 %), the mode is theoretically stable despite a hill geometry. High shear in the outer region stabilizes the mode. High beta plasma near 3 % of $<\beta>$ is in a low n mode unstable regime theoretically. Magnetic fluctuations with mode numbers (n/m=1/1, 2/2, 3/3) have no threshold $<\beta>$ value for their excitation and the fluctuation amplitudes are still increasing with $<\beta>$ within the present operational range. The observed magnetic fluctuations do not lead to any serious MHD phenomena which degrades the global energy confinement time since the confinement time still follows the ISS95 scaling even when $<\beta>$ ~ 3%. It is significant and very encouraging that the MHD stable plasma up to 3 % of $<\beta>$ is maintained in the inward shifted configuration, which has good transport properties.

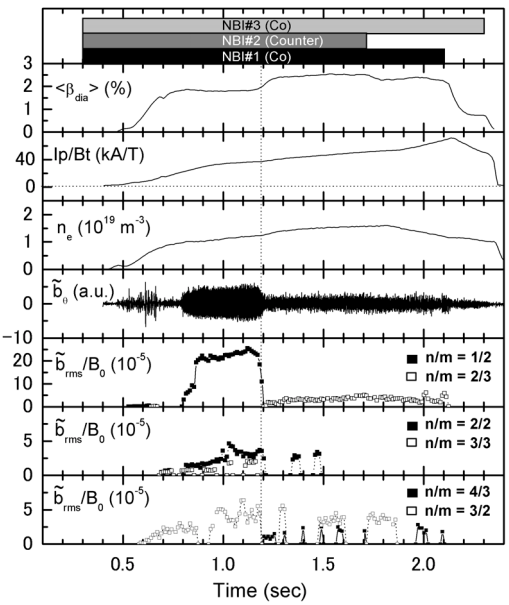

Fig. 6 With positive plasma current, MHD activities disappear at high beta.

Figure 6 shows an interesting observation that the MHD activities, monitored by the magnetic probes disappear at high beta [27]. In this discharge with R_{ax} = 3.5 m (strong hill geometry), the positive plasma current is driven by co-beam and bootstrap currents. With increasing current in time, the magnetic fluctuations suddenly disappear at t = 1.2 s ,which corresponds to the timing of the disappearance of the $\iota/2\pi = 1$ surface from the plasma region. The fluctuation amplitude with n/m =1/2 drops to near zero, as expected. But at the same time the mode amplitude with n/m = 1/1resonant mode decreases significantly and the β-value increases from 1.9 to 2.4 %. This appears to cause an increase in the pressure gradient in the outer region and hence improvement of the global confinement. This phenomenon occurs when I_p/B > 25 kA/T. It is puzzling that higher pressure gradients, a source of the pressure driven MHD mode stabilize the MHD activities.

3.2 Dynamics of the externally imposed island(n/m=1/1)

In the toroidal systems, formation of an island is a major concern since it degrades the confinement and sometimes leads to a plasma disruption. We find that the width of the island (n/m=1/1) (w: island full width in terms of ρ) varies depending upon the plasmas [28-31]. In our experiment, the width of the vacuum island, i.e., that without plasma (w_{ex}) is determined mainly from a perturbation field by the correction coils and partly from the error field. Local flattening is seen in the T_i, T_e ,E_r and n profiles around the $\iota/2\pi$ =1 surface. The width (w) is estimated by measuring that of the flattening.

The parameter space for the island suppression for a case (R_{ax} = 3.6 m, w_{ex} = 0.085, B = 2.8 T) is shown in Fig. 7 [29]. The temperature and density at the $\iota/2\pi = 1$ surface are thought to be the important parameters for the island suppression mechanism. The points (•) correspond to the cases with no detectable island (which means that $w < 0.5\ w_{ex}$) and the points (•) correspond to those with a clear island with $w \geq w_{ex}$. Suppression of the island occurs in the higher electron temperature and lower density region (region II). Instead of electron temperature and density, it may be more appropriate to use the dimensionless

quantities β and ν* [=ν_{ee} (2π/ι) (R/v_e^{th})($Z_{eff}/\varepsilon^{3/2}$)] at ι/2π = 1. Data obtained so far shows that the collisionless (ν*< 1) and finite β (> 0.1 %) plasma suppresses the island, hopefully leading to stabilization of the most unstable mode (n/m=1/1), which appears at high beta. On the other hand, a significant enlargement of the island ($w \geq 2w_{ex}$) occurs when the plasma parameter is located far to the right in the region III (i.e., collisional finite beta plasma). But we also find that this enlargement is avoided by making the vacuum island small ($w_{ex} < 0.04$) by the external simple perturbation coils. This is an important observation since the accuracy of the whole coil system required for fabrication and installation of the helical devices is substantially relaxed with a simple set of correction coils.

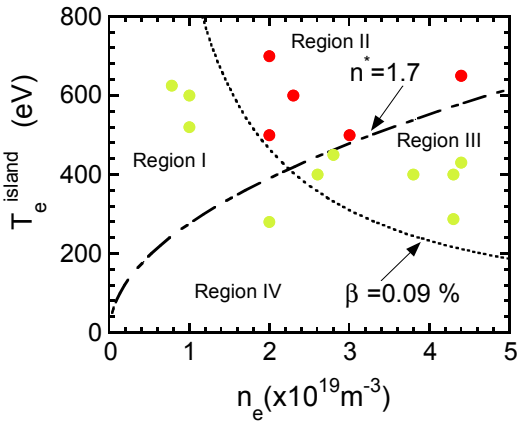

Fig. 7. Parameter space ($T_{e(island)}$, n) for island suppression for the case (w_{ex}= 0.085, B = 2.5-2.75T, R_{ax} = 3.6m). • no detectable island. • island with $w \geq w_{ex}$ Island suppression occurs in region II.

According to neoclassical tearing mode theory, positive bootstrap current modified by the island structure causes suppression of the island when dι/dρ >0 as in LHD. The bootstrap current flows significantly only when ν* < 1, consistent with the above experimental condition for the suppression. The main uncertainty is whether the bootstrap current flows in the positive direction at the ι/2π =1 surface even though we observe positive total bootstrap current. In the hill geometry, Pfirsh-Schluter current modified by the island structure tends to enlarge the island. The island enlargement occurs in the collisional plasmas in the inward shifted configurations. It is not seen in the configuration with a weaker hill geometry such as R_{ax} =3.75 m.

4. Towards Steady State Operation

Demonstration of steady-state plasma with high performance is one of the most challenging issues in developing a fusion reactor and is one of the major goals in the LHD programs. There are two key ingredients in our program of steady state operation, ICRF heating, which provides near steady state (~1h) heating power, and the divertor which handles the heat load and controls particle recycling. In this section, the research status of these areas and long pulse operation are reviewed.

4.1. ICRF Heating

The ICRF (Ion cyclotron range of frequency) heating experiment on the LHD was carried out successfully, proving that plasma characteristics particularly confinement properties between the ICRF heated and NBI heated plasmas are similar [32-34]. One of keys to the successful ICRF heating is the employment of the inward-shifted configuration with good particle orbit, i.e., R_{ax}=3.6m. High energy ions are produced by the ICRF electric field and its energy is transferred to the bulk plasma. The plasma is sustained by the ICRF heating power only. The optimum ICRF heating is found at the normalized frequency of ω/ω_{ci0}=0.9, in terms of two physical parameters; one is the enhancement factor of the confinement time normalized by ISS95, τ_E/τ_E^{ISS95}. The other is the heating efficiency, which is defined as the ratio of the absorbed RF power to the radiated power from the loop antennas. Here the applied frequency is f=ω/2π=38.47MHz and ω_{ci0} is the cyclotron frequency at the magnetic axis. For ω/ω_{ci0}=0.9 the cyclotron resonance is located on the saddle point of the mod-B surface. The

value of τ_E/τ_E^{ISS95} was 1.5. The heating efficiency reached its maximum of 80~85% [33,35]. The maximum RF power of 2.7MW is injected to the plasma using five loop antennas and the discharge with the maximum plasma stored energy (240kJ) is obtained at the electron density of $n_e = 1.4 \times 10^{19} m^{-3}$.

The confinement characteristics of high energy ions between the inward-shifted (R_{ax} = 3.6m) and the standard (R_{ax} =3.75m) configurations are examined. In Fig. 8, the measured tail temperature (T_{tail}) and the effective temperature (T_{eff}) are plotted where T_{eff} is the temperature calculated by Stix's formula, i.e., one without high energy particle loss. The ratio (T_{tail} / T_{eff}) is a good indication of the confinement of high energy ions, accelerated by an RF field. We proved experimentally the prediction of the orbit calculation, that the high energy ions are well confined in the inward-shifted configuration. On the other hand, the confinement in the R_{ax} =3.75m configuration is not satisfactory [36]. These experimental data give the transfer efficiency, which is defined as the ratio of the power transferred to the bulk plasma to the power absorbed by the high energy ions. These data are in good agreement with those of the Monte Carlo simulation [37,38]. These results indicate that ICRF heating of 10MW, planned in the near future is expected to be very effective in heating the plasma with the electron density higher than $4 \times 10^{19} m^{-3}$ for the case of 7% minority ion concentration.

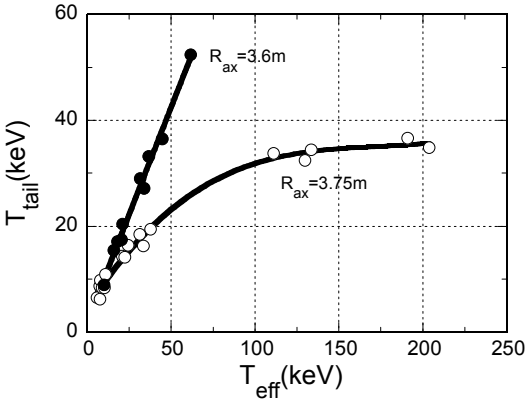

Fig.8. Relation between T_{tail} and T_{eff} at R_{ax}=3.6m and 3.75m.

4.2. Divertor

The LHD is equipped with an intrinsic built-in divertor structure [39]. Normally it is operated with an open divertor configuration. In 1999, the carbon tiles were installed as divertor plates, resulting in a significant reduction in metal impurity (Fe). Since the LHD divertor magnetic configuration has a three-dimensional structure, i.e., the divertor/ SOL structure is not a simple layer as in a tokamak. Numerical field line tracing predicts that split layers with a few cm gap strike the divertor plates at some locations. Our probe measurements clearly confirms such a structure clearly[40]. The divertor temperature ($T_{e\,div}$) and density (n_{div}) measured by probes on the divertor plates were typically 5-40 eV and $0.1 - 5.0 \times 10^{18} m^{-3}$, respectively. In Fig. 9, they are shown together with the temperature and density in the vicinity of the LCFS (n_{LCFS}, $T_{e\,LCFS}$) as a function of the average density[41]. The electron densities (n_{LCFS}, n_{div}) are about a half of the average density (n) and 1/10-1/30 of n, respectively. These linear relations are insensitive to variation in input power. The electron temperatures at the LCFS and divertor ($T_{e\,LCFS}$, $T_{e\,div}$) decrease gradually with line average density (n). The ratio of $T_{e\,div}$ to $T_{e\,LCFS}$ is approximately 0.2 and almost independent of the density. We also find that the temperature ratio remains almost unchanged when the absolute value of the temperature is increased by higher power. As described above, the shape of the temperature profile is close to parabolic in the plasma-confining region and thus the Te profile stiffness approximately holds in the entire region from the center of the discharge to the divertor plates. The configuration with R_{ax} =3.6m is surrounded by a thinner ergodic layer with a thickness of ~10 cm near the X-pont. In this configuration, $T_{e\,LCFS}$ and $T_{e\,div}$ decreases gradually with n up to $n = 9 \times 10^{19} m^{-3}$ and at this timing, the radiative power suddenly increases and both temperatures drastically drop. There is no sign of a high recycling divertor plasma or stable detached divertor plasma, which is often observed in the tokamaks. On the other hand, a plasma somewhat similar to a detached plasma is seen near the plasma thermal

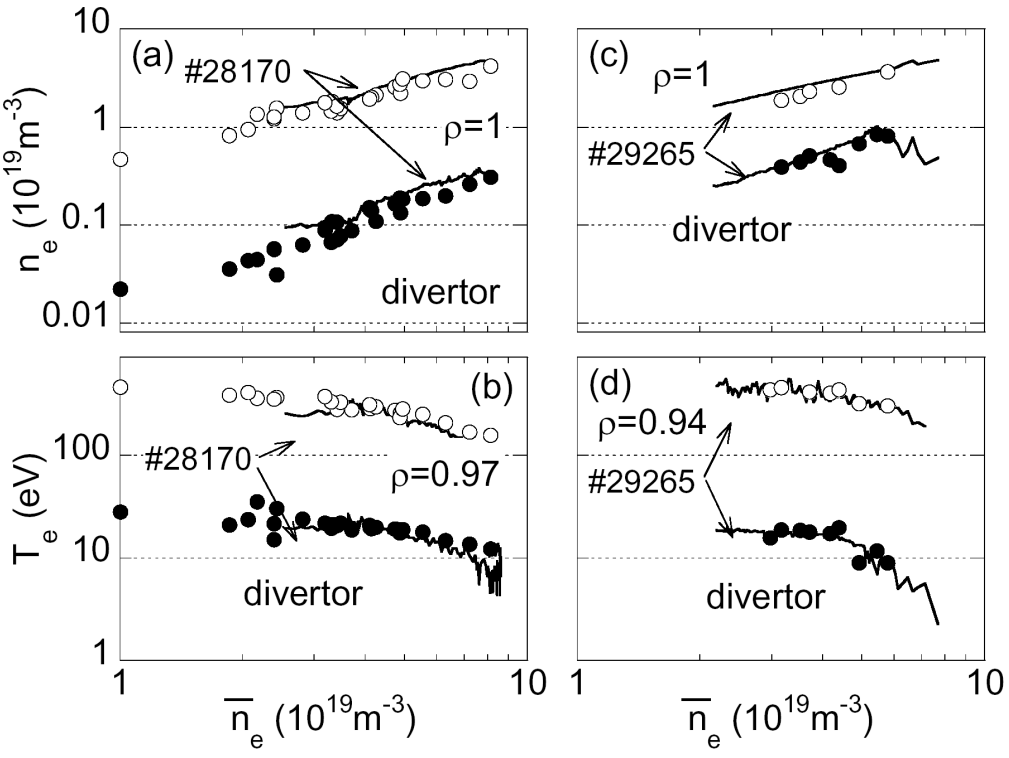

Fig.9. Electron densities (a)(c) and temperatures (b)(d) at the divertor and at LCFS are plotted as a function of the average density (n) for two types of discharges with H2 gas puffing (R_{ax}= 3.6m (narrow ergodic layer), R_{ax}=3.75 (thick ergodic layer)). Data points (• ,o) are those at the peak of the stored energy (W_p) in many discharges.

collapse in the configuration of R_{ax} = 3.75 m, which has thicker ergodic layer of ~25cm near the X-point. Near the density limit, both the divertor density and temperature start to drop.

4.3 Long Pulse Discharges

Demonstration of steady-state plasma with high performance is one of the most challenging issues in developing a fusion reactor. Such an investigation is particularly appropriate for the superconducting Large Helical Device research program[42]. The NBI (0.5 MW) heated plasma is sustained up to 80 s and an ICRF (0.4 MW) heated plasma with the discharge duration of 2 minutes is achieved. In both discharges with helium gas puffing, the electron densities are maintained at around 1 x 10^{19}m^{-3} and the temperatures are more than 1 keV during the discharge. The radiation power is less than 25 % of the input power and there is no sign of impurity accumulation. As to the operational density limit in long pulse discharges, high-density plasma with 6.7 x 10^{19}m^{-3} is sustained for 10 s with an NBI power of 2 MW. The global energy confinement characteristics of long-duration plasmas are almost the same as those in short-pulse discharges. Impurity transport is also studied using long pulse discharges with constant density and ones with slow density ramping. We find that there is a certain range of density, at which the intrinsic impurity ions accumulates in the core with a long time constant of ~10 s. The radial electric field seems to be responsible for the change of the transport [43,44]. In the near future, we have a plan to operate one-hour discharges with an input power of 3 MW. High power handling will be demonstrated together with particle control and heat removal.

5. Summary

We have made significant progress in achieving the plasma parameters with high performance [W_p (stored plasma energy) = 1.2 MJ, $T_e(0)$ = 10 keV, $<\beta> \sim 3.2$ %] during the first four years of the LHD experiment. The most important finding is that good MHD stability and favorable transport are compatible in the inward shifted configuration (R_{ax} = 3.6m). This configuration has a magnetic hill geometry and thus was predicted to be MHD unstable by ideal linear MHD stability theory. However, the plasma produced is stable at least up to $<\beta> = 3$ %. This configuration has also good orbit properties and consequently low neoclassical transport. Furthermore the observed energy confinements is a factor of 1.5 higher than that predicted by the ISS95 scaling, which means that anomalous heat diffusivity is also low. This is attributed to a high edge temperature, which is comparable to those of H-mode tokamaks. The shape of the electron temperature profile (from plasma center to divertor) is rather insensitive to variations in density and input power. With the central deposition of ECH power, however, a very peaked temperature profile (ITB) appears, providing encouragement to confinement improvement efforts. The other important achievements and observations are (i) a long pulse discharge with a duration time of 2 minutes (80 seconds) has been achieved with 0.4 MW ICRH (0.5 MW NBI) power. (ii) The externally imposed island (n/m=1/1) has a tendency of being suppressed by collisionless finite beta plasmas. (iii) ICRF heating (minority ion heating) has been very successful and the heating efficiency is comparable to that of NBI heating. (iv) The transition from ion root to electron root is seen in the low density beam heated discharges. It is confirmed that the ion thermal diffusivity is reduced by the radial electric field. (v) The divertor is very effective in preventing impurity contamination. The divertor field line structure, unique to the heliotron type configuration, has been confirmed by measuring the divertor plasma by electrostatic probes. The obtained data from the recent LHD experiment are stimulating us to propose the next step of the experiment which aims at clarifying the properties of the currentless steady state toroidal plasmas.

Acknowledgements

The authors would like to gratefully acknowledge the continuous efforts of the engineering and technical staff at NIFS and the collaborative research with participants from domestic and foreign universities, institutes and laboratories.

References

[1] A. Iiyoshi, M. Fujiwara, O. Motojima, et al., Fusion Technol. 17 , (1990)169.
[2] A. Iiyoshi, A. Komori, A. Ejiri, et al., Nucl. Fusion, 39, (1999)1245.
[3] O. Motojima et al., Nucl. Fusion, 40 (2000) 599.
[4] O. Motojima, H. Yamada. A. Komori, et al., Phys. Plasma 6, (1999)1843
[5] M. Fujiwara, K. Kawahata, N. Ohyabu et al., Nucl. Fusion, 41, (2001)1355.
[6] N. Ohyabu, A. Fujisawa, N. Ashikawa et al., Phys. Plasmas 7, (2000)1802.
[7] K. Kawahata, N.Ohyabu O.Kaneko, et al., Plasma Phys. Control. Fusion 42, (2000)B51.
[8] A, Komori, N. Ohyabu, H. Yamada, et al., Phys. Plasmas 8, (2001)2002.
[9] H. Yamada et al., Nucl. Fusion 41, (2001) 901.
[10] O. Kaneko, A. Komori, H. Yamada, et al., Phys. Plasmas 9 (2002) 2020.
[11] S. Kubo, T. Shimozuma, H. Idei et al., Journal of Plasma and Fusion Research, 78 (2002) 99.
[12] T. Shimozuma, 12th Joint Workshop on ECE and ECRH, paper No. 056 (2002).
[13] S. Okamura et al., Nucl. Fusion, 35, 283 (1995).
[14] S. Murakami, A. Wakasa, H. Maassberg, et al., Nuclear Fusion 42 (2002) L19..

[15] O. Kaneko, Y. Takeiri, K. Tsumori, et al., Nucl. Fusion, 39, 1087 (1999).
[16] U. Stroth, M. Murakami, H. Yamada et al., Nucl. Fusion 36, 1063 (1996).
[17] H. Yamada et al.,. Plasma Phys. Control. Fusion 44 (2002) A245.
[18] N. Ohyabu, K. Narihara, H. Funaba et al., Phys. Rev. Let., 84, 103 (2000).
[19] H. Yamada, K. Y. Watanabe, S. Sakakibara, et al., Phys. Rev. Lett. 84, 1216 (2000).
[20] H. Yamada et al., Plasma Phys. Control. Fusion 43 (2001) A55
[21] F. Ryter, J. Stober, A. Stabler, et al., Nucl. Fusion 41 (2001) 537.
[22] N. Ohyabu et al., to be submitted to Phys. Rev. Lett. (2002).
[23] K. Ida, H. Funaba, S. Kado, et al., Phys Rev. Lett., 23, (2001)5297.
[24] A Fujisawa, H. Ichiguchi, T. Minami, et al., Phys. Rev. Lett. 82, (1999) 266.
[25] S.Sakakibara et al., Plasma Physics and Controlled Fusion. 44 (2002) A217.
[26] A. Cooper, Plasma Phys. Control. Fusion 34 (1992) 1011.
[27] S. Sakakibara, K.Y. Watanabe, H. Yamada et al., in the Proc. Internatinal Conf. Plasma Phys., Sydney (2002)
[28] K. Narihara et al., Phys. Rev. Lett. 87 (2001) 135002.
[29] N.Ohyabu et al., Phys. Rev. Lett. 88 (2002) 055005.
[30] K. Tanaka et al., Plasma Phys. Control. Fusion 44 (2002) A231.
[31] Ida et. al., Phys. Rev. Lett. 88 (2002) 015002.
[32] T. Watari, T. Mutoh, R. Kumazawa, et al., Nucl. Fusion 41, 325 (2001).
[33] R. Kumazawa et al., Physics of Plasmas, Vol. 8 , pp. 2139-2147 (2001).
[34] T. Mutoh et al., Phys. Rev. Let., 85, (2000) 4530.
[35] K. Saito et al., Plasma Phys. Contol. Fusion 44 (2002) 103.
[36] Kumazawa R. et al., Proc. 29th Eur. Conf. Montreux, P-5.(2002) 064,.
[37] M.Sasao, S.Murakami, M.Isobe, et.al., in Proc. 18th IAEA Fusion Energy Conf. (Sorento, 2000), IAEA-CN-77/EX9/1.
[38] S. Murakami et al., Nucl. Fusion **39** (1999) 1165.
[39] N. Ohyabu, T. Watanabe, H. Ji et al., Nucl. Fusion 34, (1994) 387.
[40] S. Masuzaki, T. Morisaki, N. Ohyabu, et al., Nucl. Fusion. 42 (2001)750.
[41] S. Masuzaki, et al., to be published in J. Nucl. Mater. (2003).
[42] N. Noda et al., Nucl. Fusion, 41, (2001) 779.
[43] Y. Nakamura et al., IAEA-CN-94/EX/C5-1, this conference.
[44] Y. Nakamura et al., Plasma Phys. and Control. Fusion. 44 (2002) 2121.